Particle Detection on Low Contrast Image of Large Aperture Optics

Wendong Ding, De Xu, Zhengtao Zhang and Dapeng Zhang

Institute of Automation, Chinese Academy of Sciences, Beijing 100190
E-mail: de.xu@ia.ac.cn

Abstract: It's a challenge to identify actual deposited particles from the acquired optics image mixed with large noises. Due to the long working distance constraint for online inspecting large aperture optics, the vision system has great depth of view. It results in that the acquired optics image is blended with stain contamination on the back side of the inspected optics surface. In this paper, we propose a particle detection method for the low contrast image of large aperture optics. The method consists of three steps including particle candidate detection, image alignment and particle determination. The particle candidate detection algorithm combines the gradient information to detect small particles. The actual particles are determined by the subtraction of the reference image from the inspected image with the topological information. For the detected particle, this paper also gives a classification method to identify dust and defect. Experiment shows that the actual particle on the low contract image of large aperture optics can be effectively detected and classified with the proposed method.

Key Words: Particle inspection, image alignment, reference image subtraction, classification.

1 INTRODUCTION

Particulate contamination deposition on the Large Aperture Optics Surface (LAOS) has a serious influence on LAOS's cleanliness and results in particle induced damage on LAOS [1]. Particulate contamination initiates damage on both bare and coated optical surfaces in the presence of high intensity laser light. The decrease of cleanliness level of optics surface not only causes damage on the optics but also reduces the load capacity of optical systems which deploy a large number of optics. Quantitating particles of large aperture optics surface precisely is important for evaluating and sustaining the cleanliness level of optics and finally raising the longevity of optics.

Online particle detection and counting are particularly challenging problems due to the particle's microsize and optic's large aperture [2]. The common used method of quantitating the surface cleanliness level is realized by technician's sampling and estimation. Scanning Electron Microscopes (SEMs) and Atomic Force Microscopes (AFMs) are not effective and have limited Field Of View (FOV). They are suitable for observing the micro structure of particles not for particle aggregation.

Compared to the above mentioned method, vision based inspection method is automated, non-destructive testing and able to avoid the particle contamination induced by the measurement process considering that people are believed to be the most significant source of contamination within the contamination control community. However, the existed automated inspection instrument for large optics usually aims at the defects or scratch [3-5]. There is little literature investigating the automated inspection method of particle aggregation on large aperture optics.

Automated particle detection system is usually designed for monitoring critical locations in a cleanroom (e.g. the particle deposition is serious where the optics is face-up). Given an image of the particles deposited on optics surface, we can make statistics about the number, length, width and area of the particles. When the system measures at the certain fixed location, it can monitor the changes every 10 minutes or more.

The remainder of this paper is organized as follows. Section 2 introduces the optics surface particle inspection system. We also propose a gradient-based particle detection algorithm. A particle determination step is presented in section 3 to remove the false particles in the result of the particle candidate detection. A Binary Robust Invariant Scalable Keypoints (BRISK) detector is used to make image alignment before subtraction of the reference image from the inspected image. A classifier is trained for classifying the dust and defects in detected particles in section 4. Section 5 describes the experiment result and error analysis. Finally this paper is concluded in section 6.

2 Particle detection algorithm

The inspection system structure sketch is shown in Fig. 1. It consists of light sources and a vision system. The light sources are fixed at both sides of large optics and slightly higher than optics surface, so the incident light beams have small angle of grazing incidence. The vision system consists of a lens with changeable magnification factor and a high definition Charged Couple Device (CCD). The vision system is installed at the viewing window and its optical axis is vertical to the optics surface.

The optics surface inspecting system uses a line light source to give the small grazing incidence light illumination. The illumination way forms a dark-imaging system. Due to the airtight chamber circumstance, the stray light from the light source causes that stain contamination on the back side of the optics is imaging on the CCD. The example of acquired image is shown in Fig. 2.

Particle potential candidate detection comprises three steps. A gradient-based edge detection filter is constructed and

This work is supported by National Nature Science Foundation under Grant 61473293, 61227804 and 61303177.

used as the saliency criterion for identifying particle candidates. As a matter of fact, the pixel area of a particle ranges from single pixel to cluster of pixels. Here we constructed an edge detection filter.

$$\mathbf{I}'_s = \frac{1}{Z_s}\sum_{t\in\Omega} g(|\nabla \mathbf{I}_t|;\sigma_s)\mathbf{I}_s \qquad (1)$$

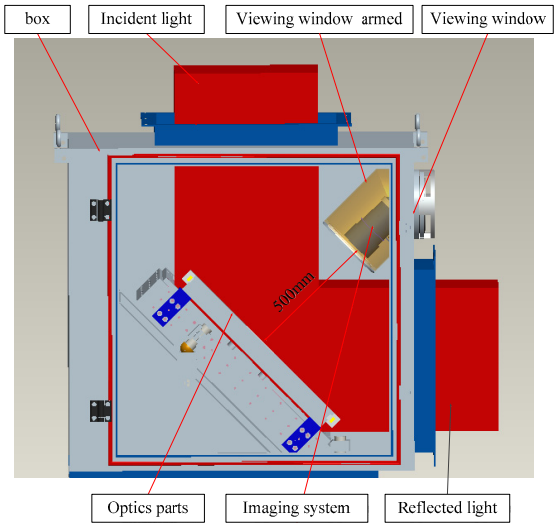

Fig. 1 The inspection system structure is inside an airtight chamber. The red area is the space scope of intrinsic light path of optical system which the inspected optics belongs to.

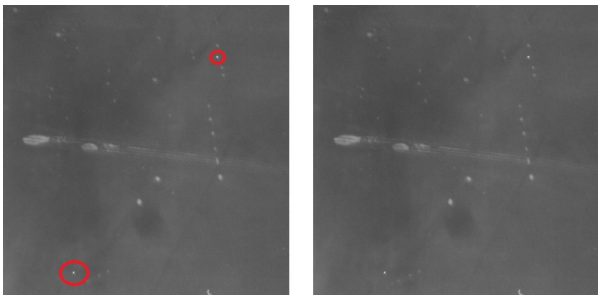

Fig. 2 Example particle image. In left sub-image, the objects selected by red circle are actual particles, while other bright regions in the image are stain contamination in the other side of the optics.

where $\mathbf{I}'_s$ is the filtered output at pixel s, Ω denotes the set of pixels t in the window which is centered at s, and $g(x;\sigma)$ is a Gaussian function with variance σ^2. Z_s is the normalization term, which is calculated as $Z_s = \sum_{t\in\Omega} g(|\nabla \mathbf{I}_t|;\sigma_s)$. $|\nabla \mathbf{I}_t|$ is the magnitude of the image gradient. Different from the box filter, the pixel-based filter is more suitable for the small particle existence condition. In fact, small particles will vanish if the rectangle mean method is used.

In the second step, we classify each pixel i to particle's edge if:

$$\mathbf{I}_s - \mathbf{I}'_s \geq \varepsilon_1 \qquad (2)$$

Where ε_1 is positive value, it controls the sensitivity of the algorithm to the particle. Here we only filter out the edge of the particles, based on (2), the whole particle region's pixel is

$$\mathbf{R}_p = \{s \,|\, \mathbf{I}_s \geq \mathbf{I}_e \;\; \&\& \;\; (\exists\, t \text{ s.t. } \mathbf{I}_t \geq \mathbf{I}_e \;\; \&\& \; t \in U_4(s))\} \qquad (3)$$

Where $U_4(s)$ is 4-nearest neighborhood of s, $\mathbf{I}_e$ is the edge pixel of particles. (3) gives a recursive criterion to generate the whole particle region.

When the distances between the corresponding points are less than a special value, ε_2, they are ε-neighborhood[6]. If $d(t_1,s) < \varepsilon_2 \;\; \&\& \; d(t_2,s) < \varepsilon_2$, then $t_1, t_2 \in U(s)$. Some particles are split into several divergent connection regions. We cluster them based on the position information.

$$\begin{aligned} &\text{if} \quad t_1 \in \mathbf{R}_p^1 \quad \&\& \quad t_2 \in \mathbf{R}_p^2 \quad \&\& \quad t_1, t_2 \in U(s) \\ &\text{then} \quad s \in \mathbf{R}_p \end{aligned}$$

Then pixel s is partitioned into the particle region. The particle regions $\mathbf{R}_p^1$ and $\mathbf{R}_p^2$ finally are clustered into connected region.

3 Particle confirmation

3.1 Alignment of the corresponding particles

Although we detect out the particle candidates in the previous step, not all these candidates are actual deposited particles. In this step the actual particle is identified by the subtraction of the reference image from the inspected image. As shown in Fig. 3, all the particle candidates detected by our method contain both actual particles and false ones.

After we have got the particle potential candidates, the next step is to select out the actual particles. Alignment between inspection image and reference image is a prerequisite for the generation of subtraction result to find particles by comparing them.

Suppose that $\mathbf{M} = [X, Y, 0]^T$ is a point on the optics surface. $\mathbf{m}_1 = [u_1, v_1]$ and $\mathbf{m}_2 = [u_2, v_2]$ are the image points correspond to image project $\mathbf{M}$ in the inspected image and reference image. Their augment vector by adding 1 is $\tilde{\mathbf{M}} = [X, Y, 0, 1]^T, \tilde{\mathbf{m}}_1 = [u_1, v_1, 1]^T, \tilde{\mathbf{m}}_2 = [u_2, v_2, 1]^T$. A camera is modeled by the usual pinhole: the relationship between a surface point $\tilde{\mathbf{M}}$ and its image projection $\tilde{\mathbf{m}}_1$ and $\tilde{\mathbf{m}}_2$ is given by

$$\begin{aligned} \lambda_1^p \tilde{\mathbf{m}}_1 &= \mathbf{A}\begin{bmatrix}\mathbf{R}_1 & \mathbf{t}_1\end{bmatrix}\mathbf{M} \\ \lambda_2^p \tilde{\mathbf{m}}_2 &= \mathbf{A}\begin{bmatrix}\mathbf{R}_2 & \mathbf{t}_2\end{bmatrix}\mathbf{M} \end{aligned} \qquad (4)$$

where λ_i^p is an arbitrary scale factor. $(\mathbf{R}_i, \mathbf{t}_i)$ is called the extrinsic parameters. They are the rotation and translation which relate the world coordinate system to the camera coordinate system. $\mathbf{A}$ is called the camera intrinsic matrix.

Based on the projection model in (4), we can get

$$\lambda_i^p \begin{bmatrix} u_i \\ v_i \\ 1 \end{bmatrix} = \mathbf{A}\begin{bmatrix} \mathbf{R}_i & \mathbf{t}_i \end{bmatrix} \begin{bmatrix} X \\ Y \\ 1 \end{bmatrix}, i = (1,2) \tag{5}$$

Here suppose

$$\begin{bmatrix} u_2 & v_2 & 1 \end{bmatrix}^T = \mathbf{H}\begin{bmatrix} u_1 & v_1 & 1 \end{bmatrix}^T \tag{6}$$

then

$$\mathbf{H} = \frac{\lambda_2^p}{\lambda_1^p}\mathbf{A}\begin{bmatrix} \mathbf{R}_2 & \mathbf{t}_2 \end{bmatrix}\begin{bmatrix} \mathbf{R}_1 & \mathbf{t}_1 \end{bmatrix}^{-1}\mathbf{A}^{-1} \tag{7}$$

$\mathbf{H}_{3\times3}$ is the homography matrix, it has 8 independent parameters. Suppose

$$\mathbf{H} = \begin{bmatrix} c_{00} & c_{01} & c_{02} \\ c_{10} & c_{11} & c_{12} \\ c_{20} & c_{21} & c_{22} \end{bmatrix} \tag{8}$$

substitute (8) into (6), we can get

$$u_2 = \frac{c_{00}u_1 + c_{01}v_1 + c_{02}}{c_{20}u_1 + c_{21}v_1 + c_{22}} \tag{9}$$

$$v_2 = \frac{c_{10}u_1 + c_{11}v_1 + c_{12}}{c_{20}u_1 + c_{21}v_1 + c_{22}} \tag{10}$$

rewrite it we can get

$$\begin{cases} c'_{00}u_1 + c'_{01}v_1 + c'_{02} - c'_{20}u_1u_2 - c'_{21}v_1u_2 = u_2 \\ c'_{10}u_1 + c'_{11}v_1 + c'_{12} - c'_{20}u_1v_2 - c'_{21}v_1v_2 = v_2 \end{cases} \tag{11}$$

where $c'_{ij} = c_{ij} / c_{22}$ $(i, j \in \{0,1,2\})$. For $n \geq 4$ given known points, $\mathbf{H}$ can be determined by (11).

To find the matched point pairs, we use Binary Robust Invariant Scalable Keypoints (BRISK) to detect the keypoints and find the matched point pairs.

BRISK detector detects keypoints in octave layers of the image pyramid as well as in layers in-between. The octaves are obtained by progressively half-sampling. Initially, the Features from Accelerated Segment Test (FAST) detector [7] is applied in this algorithm on each octave and intra-octave separately using the same threshold T to identify potential regions of interest. Then, a non-maxima suppression method is performed to find the extreme point. The method performs a sub-pixel and continuous scale refinement for each detected maximum. The location and the scale of each keypoint are obtained in the continuous domain.

BRISK descriptor estimates the direction $\mathbf{g}$ of the keypoint. Then it applies the sampling pattern rotated by $\alpha = \arctan \mathbf{g}$ around the keypoint. Finally the descriptor assembles a bit-vector by performing intensity comparisons between each point pair.

Matching two BRISK descriptors [8-10] is a simple computation of their Hamming distance. The number of bits different in the two descriptors is a measure of their dissimilarity.

3.2 Particle determination

Considering that the particle region in the gray-scale image is presented as a bright area which makes the average intensity around the area changes greatly. The position relationship of particle regions of the reference image and inspected image may have 2 cases as below.

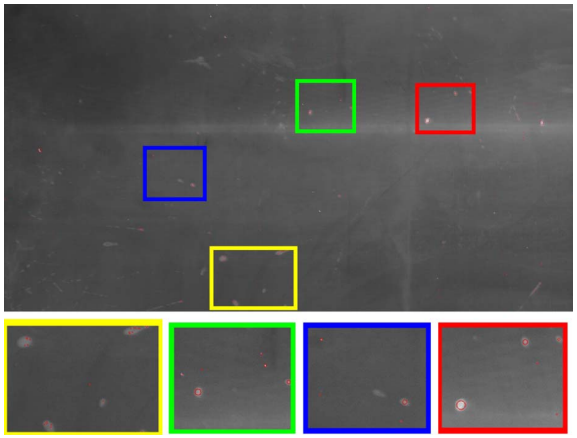

Fig. 3 Particle image detection result, all particle candidates blended with actual particles and false particles.

- Two particles are concentric or have big degree of overlap.
  - Average intensity around the area changes greatly. This means that a new particle exists in the inspected image.
  - Average intensity around the area does not change greatly. It means that no new particle exists.
- If two particle regions are non-concentric and have small degree of overlap, a new particle exists.

Let $\beta \in \mathbf{B}$ where $\mathbf{B}$ is the set of all closed, parameterized, absolutely continuous curves. Absolutely continuous, parameterized curve β is the particle contour. Let $L_\beta = \int_0^1 |\dot{\beta}(t)|\, dt$ be the length of the curve β, where the $|\cdot|$ is Euclidean 2-norm. The centroid of β is defined as $C_\beta = \frac{1}{L_\beta}\int_0^1 \beta(t)\,|\dot{\beta}(t)|\, dt$. The covariance of β is defined as $\Sigma_\beta = \frac{1}{L_\beta}\int_0^1 (\beta(t) - C_\beta)\,|\dot{\beta}(t)|\, dt$. The mean value inside the curves is $M_p = \frac{1}{N}\sum_{p\in\Gamma}\mathbf{I}(p)$ where N is the pixel number of set Γ, Γ is the set containing all the pixels inside of $\mathbf{B}$. M_{pp} and M_{pr} are the mean intensity of particle candidates in the inspected image and the reference

image, if $M_{pp} - M_{pr} > \lambda_2$, then mean intensity changes greatly.

Definition 1. Let $\mathbf{P}_i$ be particle candidate set in inspected image and $\mathbf{P}_r$ particle candidate set in reference image, and $D_{ir} = | C_i - C_r |$ where C_i and C_r are the centroids of $\mathbf{P}_i$ and $\mathbf{P}_r$. If $D_{ir} \le \lambda_1$, the candidates are concentric.

Definition 2. N_o is pixel number of $\Gamma_i \cap \Gamma_r$, N_u is pixel number of $\Gamma_i \cup \Gamma_r$. The degree of overlap $D_o = \frac{N_o}{N_u}$. If the degree of overlap of two candidates $D_o \ge \lambda_3$, two particle candidates are overlap.

In the condition of overlap, there are two cases, the contours of two candidates are intersected, one contour is fully inside the other contour. The former can be detected by the polygon intersection calculation algorithm. Polygon intersection calculation is implemented by enumerating the line segment intersection. It clockwise queues the cross points along the sides to make sure that the curve is closed. The latter needs to test whether all the corner points of one candidate are inside the other.

4 Particle classification

In the above content, we only describe how to extract the particles. In fact, particles on optics include both dust and defects. In this paper, we give a machine learning algorithm to identify the dust and defects.

Dust particles on the optics surface tend to induce defects after the high intensity light pass through the surface of optics. Digs in defects are point-like in shape as dust particles. In addition, defects on optical surfaces are imperfections. They can also be formed from the manufacturing process and remanufacture. Since digs and dust particles are totally different matters, a method to discriminate digs and dust particles on the optical surfaces is needed.

There are some differences [11] between digs and dust particles in both electromagnetic scattering and generation. The gray scale distribution of the image has respective features. The dig is the trace produced by the abrasive particle during grinding. Since the abrasive particles are usually smooth and round in the process of precision manufacture, the digs are usually regular in shape. On the contrary, the forming reasons of dust are complex and multiple, and the shapes of dust vary greatly.

At the start of the particle classification, feature extraction is executed from the three aspects: histogram of gradient, texture, and morphology. Histogram of Oriented Gradient [12] is based on evaluating well-normalized local histograms of image gradient orientations in a dense grid and used for human detection. Here we use both histogram of gradient of magnitude and orientation. Features related to texture are constructed by Gray Level Co-occurrence Matrix (GLCM) from image, we use Contrast, Correlation, Energy (detail formula can be referred to [3]) to reflect image smoothness and image information. Spatial co-occurrence among features could increase the discriminative power of features.

The morphological characters are represented by invariant moment. Finally, there are 160 features for digs and dust particle classification selected in total.

In the second step, since there are large differences existed in the data scale of the features, normalization is employed. If the input sample data have too many dimensions, no matter what machine learning algorithms would cost considerable training time, the learning process is more difficult relative to the low dimension case [13]. The curse of dimension often occurs when the learning algorithm works fine in low dimension but the problem becomes intractable in high-dimension. Principal component analysis (PCA) [14] is a technique used to emphasize variation and bring out strong patterns in a dataset. It's often used to make data easy to explore and visualize. Finally, Support Vector Machine (SVM) [15] learning method is used for the training and prediction process.

To obtain good classification results, some parameters in SVM are optimized by cross validation. These parameters include (1) C, the regularization parameter, determining the trade-off between the training error and the smoothness, and (2) γ, the squared bandwidth of the Radial Basis Function (RBF) kernel.

5 Experiment Result

The computer used in the experiment system is with a 2.66 GHz processor and 8 GB of memory. The line light sources were 525mm long with blue light. The optics image was acquired before and after the status of the optics was changed (e.g. high flux laser pass, cleaning). For the parameter study, we used 30 optics images without particle as the reference image and 5 optics images with various sizes of particles. For the performance evaluation, we used another 8 optics images. The size of the image is 6600×4400 pixels and each pixel has 8-bits gray-scale intensity. The real inspection system is shown as Fig. 4.

5.1 Particle candidate detection

Due to the low-SNR nature of the optics image, we first calculated the gradient of the image, and used it to boost the edge detection of the particles. For each pixel, their immediate surrounding areas' gradient was constructed as the weight of the filter. Fig. 5a is the magnified part of the original image. Fig. 5b shows the extracted particle candidates corresponding to the image area in Fig. 5a. Three rows of the image in Fig. 5a and Fig. 5b are shown in Fig. 5c. The three rows are labeled in Fig. 5a and Fig. 5b. 1-D gray-scale distribution of the three rows demonstrates that the algorithm can detect small signal change and reject the considerable noise level. The parameters used of the algorithm is set as $\sigma = 5$, $\varepsilon_1 = 0.03$, $\varepsilon_2 = 5$, and Ω is set as 5×5 window. In fact, the weak threshold ε_1 was set the same both for the reference image and inspected image. The wrong detection would be eliminated by the subtraction algorithm.

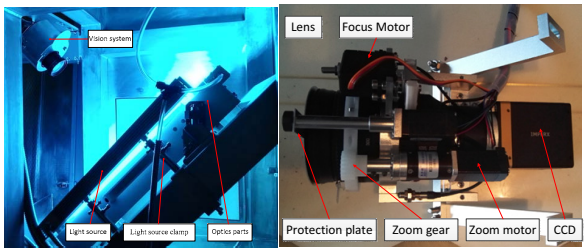

(a) (b)

Fig. 4 Real inspection system. (a) The whole inspection system and the inspected optics. (b)The vision system composition.

5.2 Particle determination

On the optics image, we generated various sizes of particles. The diameter of the particle ranged from 1 to 19 pixels. The number distribution over particle size obeyed the normal distribution as $\xi = N(\lambda_4 / \delta_i, \sigma_1^2)$. where $\lambda_4 = 100$ $\sigma_1^2 = 50$ and δ_i is the size of particle. The minimum distance $\lambda_1 = 5$, minimum lightness variance $\lambda_2 = 50$, and minimum degree of overlap $\lambda_3 = 0.1$.

These parameters were used in the real optics image experiment. Fig. 6 gives the comparison between the actual particle number and the measured result of the real optics image. It gave the particle number with the error less than 35%. Fig. 7 shows the optics image labeled with red circles at actual particles' positions.

5.3 Particle classification

The detected particle was manually divided into two sets as the training data. To evaluate the performance of the classifier, cross verification was used to determine the optimal parameters. PCA was performed on the normalized data. The Pareto chart of the ten Principle Components (PCs) is shown in Fig. 8. Clearly, the ten PCs explained much higher variance contribution rate contrast to other PCs. With the accumulative contribution rate of above 90%, the ten PCs represented most information of the digs and dust particles. The original dimension of the selected feature is shown as Table. 1. Fig. 9 gives the result of SVM classifier parameter optimization. When $C = 0.1$ and $\gamma = 10^{-5}$, the classifier had best performance, then on the test dataset the error was 5%. So the dust and defects could be distinguished by the SVM classifier.

6 Conclusion

Particle inspection in large aperture optics is a longstanding problem due to several reasons. First, the required inspected particle is too small compared to the inspection area. Second, online inspection faces with some spatial constraints which lead to difficulties to the particle inspection of the large aperture optics. Particle detection algorithm preformed only on the inspected image cannot realize accurately identifying the actual particle with the stain contamination blended in the inspected image.

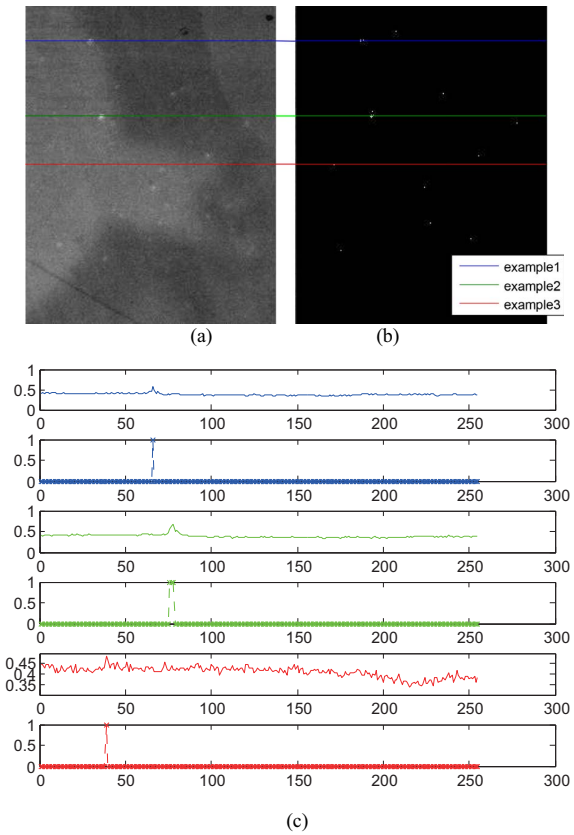

(a) (b)

(c)

Fig. 5 Particle candidate detection result. (a)Magnified part of original optics image. (b)The extracted particle candidates. Three rows of images in (a) and (b) are labeled with horizontal line, their gray value is shown in (c).

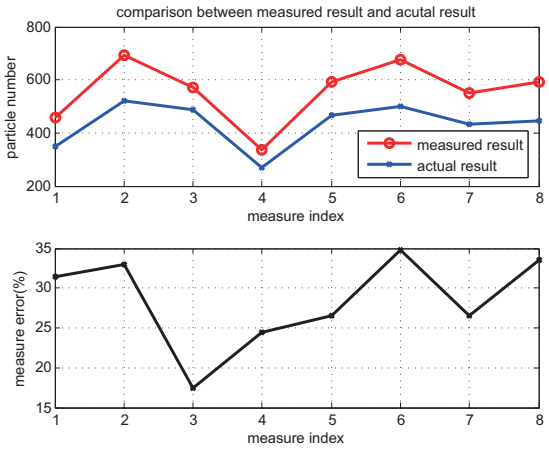

Fig. 6 Particle number counting errors.

We present a new particle inspection method. It demonstrates a good ability of detecting particles on low contract image of large aperture optics which is implemented by several steps on the inspected image. The key of proposed method is to detect all the candidates and then remove the false particles by comparison with the reference image.

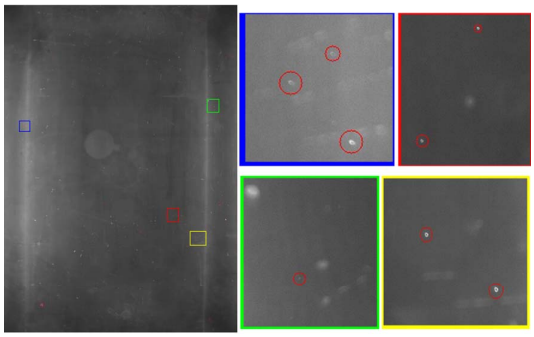

Fig. 7 The optics image labeled with red circles at actual particles' positions.

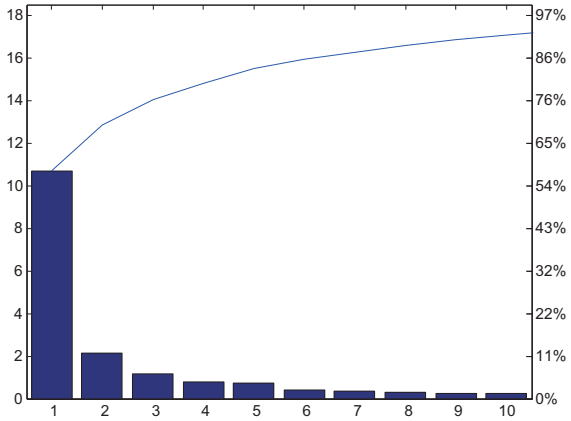

Fig. 8 Pareto Chart of the ten top features.

Table. 1 Dimensions of the selected features.

HMG	HOG	Contrast	Correlation	Energy	Moment
8	8	44	44	44	7
Area	Solidity	Orientation	mean	std	Total
1	1	1	1	1	160

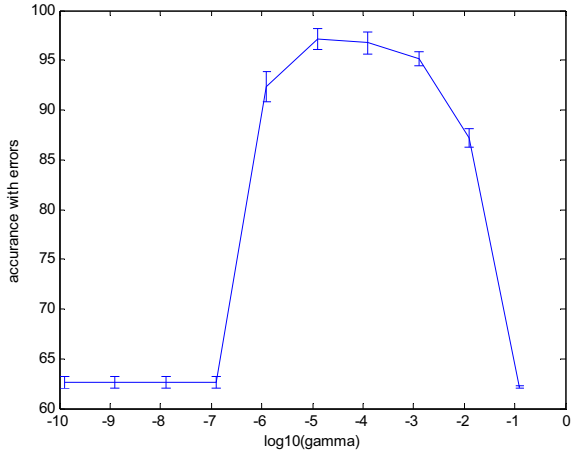

Fig. 9 SVM γ Optimization

REFERENCES

[1] A. A. Manenkov, Fundamental mechanisms of laser-induced damage in optical materials: todays state of understanding and problems, Optical Engineering, Vol. 53, No. 1, 010901, 2014.

[2] Y. Yang, S. Wang, X. Chen, L. Li, P. Cao, L. Yan, Z. Cheng, and D. Liu, Sparse microdefect evaluation system for large fine optical surfaces based on dark-field microscopic scattering imaging, in Proc. SPIE, Vol. 8838, 2013, 883 806–883 806–9, 2013.

[3] R. Shanmugamani, M. Sadique, and B. Ramamoorthy, Detection and classification of surface defects of gun barrels using computer vision and machine learning, Measurement, Vol. 60, 222 – 230, 2015.

[4] S. Kang, J. Lee, K. Song, and H. Pahk, Automatic defect classification of tft-lcd panels using machine learning, in IEEE International Symposium on Industrial Electronics, 2009., 2175–2177, July 2009.

[5] M. Antonello, S. Ghidoni, and E. Menegatti, Autonomous robotic system for thermographic detection of defects in upper layers of carbon fiber reinforced polymers, in Proceedings of 2015 IEEE International Conference on Automation Science and Engineering (CASE), 634–639. Aug 2015.

[6] U. von Luxburg, A tutorial on spectral clustering, Statistics and Computing, Vol. 17, No. 4, 395–416, 2007.

[7] E. Rosten and T. Drummond, Machine learning for high-speed corner detection, in Proceedings of the 9th European Conference on Computer Vision - Vol I, Berlin, Heidelberg: Springer-Verlag, 430–443, 2006.

[8] S. Leutenegger, M. Chli, and R. Siegwart, Brisk: Binary robust invariant scalable keypoints, in Proceedings of the 2011 IEEE International Conference on Computer Vision (ICCV), 2548–2555, Nov 2011.

[9] M. Calonder, V. Lepetit, C. Strecha, and P. Fua, Brief: Binary robust independent elementary features, in Proceedings of the 11th European Conference on Computer Vision: Vol IV, Berlin, Heidelberg: Springer-Verlag, 778–792, 2010.

[10] H. Bay, A. Ess, T. Tuytelaars, and L. Van Gool, Speeded-up robust features (surf), Comput. Vis. Image Underst., Vol. 110, No. 3, 346–359, Jun. 2008.

[11] L. Li, D. Liu, P. Cao, S. Xie, Y. Li, Y. Chen, and Y. Yang, Automated discrimination between digs and dust particles on optical surfaces with dark-field scattering microscopy, Appl. Opt., Vol. 53, No. 23, 5131–5140, Aug 2014.

[12] N. Dalal and B. Triggs, Histograms of oriented gradients for human detection, in Proceedings of the 2005 IEEE Computer Society Conference on Computer Vision and Pattern Recognition (CVPR), Washington, DC, USA: IEEE Computer Society, 886–893, 2005.

[13] P. Domingos, A few useful things to know about machine learning, Commun. ACM, Vol. 55, No. 10, 78–87, Oct. 2012.

[14] J. Shlens, A tutorial on principal component analysis, arXiv preprint arXiv:1404.1100, 2014.

[15] C. Burges, A tutorial on support vector machines for pattern recognition, Data Mining and Knowledge Discovery, Vol. 2, No. 2, pp.121–167, 1998.